

*Annual Review of Earth and Planetary Sciences*  
**Ab Initio Study on the Lower  
 Mantle Minerals**

Taku Tsuchiya, Jun Tsuchiya, Haruhiko Dekura,  
 and Sebastian Ritterbex

Geodynamics Research Center, Ehime University, Matsuyama 790-8577, Japan;  
 email: [tsuchiya.taku.mg@ehime-u.ac.jp](mailto:tsuchiya.taku.mg@ehime-u.ac.jp)

Annu. Rev. Earth Planet. Sci. 2020. 48:99–119

First published as a Review in Advance on  
 December 3, 2019

The *Annual Review of Earth and Planetary Sciences* is  
 online at [earth.annualreviews.org](http://earth.annualreviews.org)

<https://doi.org/10.1146/annurev-earth-071719-055139>

Copyright © 2020 by Annual Reviews.  
 All rights reserved

**Keywords**

ab initio density functional computation, Earth’s lower mantle bridgmanite, postperovskite, dense hydrous phase, lattice thermal conductivity

**Abstract**

Recent progress in theoretical mineral physics based on the ab initio quantum mechanical computation method has been dramatic in conjunction with the rapid advancement of computer technologies. It is now possible to predict stability, elasticity, and transport properties of complex minerals quantitatively with uncertainties that are comparable to or even smaller than those attached in experimental data. These calculations under in situ high-pressure (*P*) and high-temperature conditions are of particular interest because they allow us to construct a priori mineralogical models of the deep Earth. In this article, we briefly review recent progress in studying high-*P* phase relations, elasticity, thermal conductivity, and rheological properties of lower mantle minerals including silicates, oxides, and some hydrous phases. Our analyses indicate that the pyrolytic composition can describe Earth’s properties quite well in terms of density and P- and S-wave velocity. Computations also suggest some new hydrous compounds that could persist up to the deepest mantle and that the postperovskite phase boundary is the boundary of not only the mineralogy but also the thermal conductivity.

- The ab initio method is a strong tool to investigate physical properties of minerals under high pressure and high temperature.
- Calculated thermoelasticity indicates that the pyrolytic composition is representative to the chemistry of Earth’s lower mantle.
- Simulations predict new dense hydrous phases stable in the whole lower mantle pressure and temperature condition.
- Calculated lattice thermal conductivity suggests a heat flow across the core mantle boundary no greater than 10 TW.

ANNUAL REVIEWS **CONNECT**

[www.annualreviews.org](http://www.annualreviews.org)

- Download figures
- Navigate cited references
- Keyword search
- Explore related articles
- Share via email or social media

## 1. INTRODUCTION

Progress in computational mineral physics based on the ab initio quantum mechanical calculation method has been dramatic in the last decade in conjunction with the rapid advancement of computer technologies. While the classical molecular simulations required an empirical treatment on the interatomic model potentials, which entirely rely on available experimental data and are often oversimplified, the quantum mechanical Hamiltonian of many-body electron systems can be efficiently and quantitatively evaluated even without any empirical treatment on the basis of the density functional theory (DFT) (Hohenberg & Kohn 1964, Kohn & Sham 1965). Practical calculations of minerals having complex crystal structures can be achieved by combining various methods and techniques developed following the DFT. As a result of such advancement in the ab initio techniques, it is now possible to predict stability and several physical properties, including elasticity and thermodynamic and electronic properties, of materials under high pressure ( $P$ ) quantitatively with uncertainties that are comparable to or even less than those found in experimental data. Reliable determination of high- $P$ , high-temperature ( $T$ ) elasticity, phase stability, and transport properties—some of which are still quite difficult experimentally in the entire Earth's lower mantle condition—is of significant geophysical importance. The technique is now one of the most promising to tightly constrain the thermochemical conditions of the deep Earth.

The lower mantle (from 660 to 2,890 km depth, from 24 to 136 GPa, and from  $\sim 1,900$  to  $\sim 4,000$  K), the largest region in Earth, is generally thought to have an ultramafic peridotitic-like composition. But this leads to a substantial deficiency of Si of  $\sim 11\%$  in the bulk silicate Earth compared to the Mg/Si ratio of primitive chondrite (Wade & Wood 2005). It is therefore still under debate whether the lower mantle composition is pyrolytic or more chondritic. Direct comparisons between the calculated seismic velocities and the actual Earth's values (e.g., Wang et al. 2015) allow us to construct mineralogical models of the lower mantle. Applications of the ab initio techniques are not limited to the equilibrium properties of the major lower mantle phases. Remarkable outcomes can also be seen recently in studies on the new high- $P,T$  stability of dense hydrous phases (e.g., Tsuchiya 2013, Nishi et al. 2017), and new techniques for transport properties have been developed (e.g., Dekura et al. 2013, Dekura & Tsuchiya 2017). In this article, we review the recent progress of ab initio studies on high- $P,T$  phase relations, elasticity, thermal conductivity, and plasticity of the major lower mantle phases and some hydrous compounds.

## 2. AB INITIO METHODS FOR MINERAL PHYSICS

Ab initio approaches are those that solve the fundamental equations of quantum mechanics with a bare minimum of approximations. DFT is, in principle, an exact theory for the ground state and allows us to reduce the interacting many-electron problem to a single-electron problem (the nuclei being treated as an adiabatic background). A key to the application of DFT in handling the interacting electron gas was given by Kohn & Sham (1965) by splitting the kinetic energy of a system of interacting electrons into the kinetic energy of noninteracting electrons plus some remainder, which can be conveniently incorporated into the exchange-correlation energy. Using the variational principle, the one-electron Schrödinger equation, known as the Kohn-Sham equation, can be derived from the all-electron Schrödinger equation. Based on this, total energy of the whole system is described with kinetic energy, classical Coulomb potentials from ion cores, those between electrons, and exchange-correlation potential using charge density. The exchange-correlation potential contains all the quantum many-body effects. The local density approximation (LDA) (Kohn & Sham 1965, Ceperley & Alder 1980, Perdew & Zunger 1981) replaces the exchange-correlation potential at each point by that of a homogeneous electron gas with a density equal to the local density at the point. The LDA works remarkably well for a wide variety of

materials, especially in the calculations of equations of state, elastic constants, thermodynamics, and phonon conductivities of silicates. Cell parameters and bulk moduli obtained from well-converged calculations often agree with the experimental data within a few percent.

Attempts to improve LDA via introducing nonlocal corrections have yielded some success. The generalized gradient approximation (GGA) (Perdew et al. 1992, 1996) is a significantly improved method over LDA for certain transition metals (Bagno et al. 1989) and hydrogen-bonded systems (Hamann 1997; Tsuchiya et al. 2002, 2005). There is some evidence, however, that GGA improves the energetics of silicates and oxides, but the structures can be underbound. The volume and bulk modulus calculated with GGA tend to be larger and smaller, respectively, than those measured experimentally (Hamann 1996, Demuth et al. 1999). Considering the thermal effect with zero-point motion, LDA provides structural and elastic quantities much closer (typically within a few percent) to experimental values than those obtained with GGA. In addition, a discrepancy of about 10–15 GPa is usually seen in transition pressures calculated with LDA and GGA (e.g., Hamann 1996, Tsuchiya et al. 2004c, Dekura et al. 2011), which provide lower and upper bounds, respectively. Experimental transition pressures are usually found between the values obtained within LDA and GGA, although GGA tends to provide a  $P$  value with better fit to the experimental value than LDA (e.g., Hamann 1996; Tsuchiya et al. 2004a,c). The main source of computational error can be attributed to how to treat the exchange–correlation potential (Yu et al. 2007).

The standard DFT has limitations in applying to Fe-bearing oxides and silicates in the following case. One-electron approximation with the standard DFT approaches fails to describe the interactions between localizing electrons with strongly correlated behavior, such as  $3d$  electrons of Fe in the Fe–O system. Conventional mean-field types of treatments on the exchange–correlation potential including both LDA and GGA usually produce (semi)metallic bands or considerable underestimations of the band gap for Fe–O bonding in silicates (e.g., Tsuchiya et al. 2006a; Metsue & Tsuchiya 2011, 2012; Tsuchiya & Wang 2013). Since they also do not provide the correct crystal field effects that break the  $d$ -orbital degeneracy, more sophisticated classes of technique, such as LDA +  $U$ , LDA +  $U$  + DMFT (dynamical mean-field theory), and so on, are needed to treat the many-body effect of electrons more accurately and to investigate geophysically important Fe-bearing systems. Among these schemes, the LDA +  $U$  method (Anisimov & Gunnarsson 1991) is for now the most practical method for minerals, where the correction is applied to the onsite Coulomb interaction between Fe  $d$  states. Tsuchiya et al. (2006b), Metsue & Tsuchiya (2011, 2012), and Tsuchiya & Wang (2013) computed the effective  $U$  in  $(\text{Mg}_{1-x}\text{Fe}^{2+x})\text{O}$  ferropericlasite (Fp),  $(\text{Mg}_{1-x}\text{Fe}^{2+x})\text{SiO}_3$  postperovskite (PPv) and bridgmanite (Br), and  $(\text{Mg}_{1-x}\text{Fe}^{3+x})(\text{Si}_{1-x}\text{Fe}^{3+x})\text{O}_3$  Br, respectively, nonempirically based on an internally consistent linear response approach (Cococcioni & de Gironcoli 2005). Presently, the ab initio LDA +  $U$  technique is a quite important technique to investigate the physical properties of Fe-bearing systems relevant to Earth's deep interior.

Elastic constant tensor for a single crystal can be calculated with high precision in a method described briefly below. Combined with the ab initio planewave pseudopotential method, pioneering works by Karki et al. (1997a–c) and Karki & Crain (1998) applied the technique to determine the elasticity of major mantle minerals of MgO, SiO<sub>2</sub>, MgSiO<sub>3</sub> Br, and CaSiO<sub>3</sub> Pv as a function of  $P$ . Direct comparison between the ab initio and seismological elasticity now spawns a new line of geophysical research. Determination of the elastic constants by means of the DFT simulation proceeds as follows: (a) At a given pressure (or volume) the crystal structure is first fully optimized. (b) The lattice is slightly deformed by applying a small strain, and the stress in the strained configuration is calculated. The values of the elastic constants are determined from the linear stress–strain relation or quadratic energy–strain relation. In these calculations, the ionic positions need to be reoptimized in the strained lattice to incorporate any couplings between strains and

vibrational modes in the crystal (Nastar & Willaime 1995), and the elastic constants need to be computed in the appropriate limit of zero strain. To calculate the elastic constants in the linear regime, which is appropriate for the geophysical condition, strains of different magnitude or sign are applied, and the zero-strain limit is determined by interpolation. After obtaining the single crystal elastic constant tensor, polycrystalline isotropic elasticity, bulk ( $K$ ), and shear moduli ( $\mu$ ) are bounded based on relevant averaging schemes. Although the most appropriate method is still unclear for the geophysical condition, the most often applied one is the Voigt–Ruess–Hill average (Hill 1952) or Hashin–Shtrikman average (Hashin & Shtrikman 1962). The isotropic averaged compressional ( $V_P$ ) and shear ( $V_S$ ) wave velocities can then be calculated using as aggregate  $K$  and  $\mu$  moduli. Combining this technique and ab initio free energy calculation methods based on the lattice dynamics (LD) method (Baroni et al. 1987) and quasiharmonic approximation (QHA) (Wallace 1972), researchers successfully extended the condition to finite  $T$  by including phonon thermodynamics (Karki et al. 1999; Wentzcovitch et al. 2004, 2006; Wang et al. 2015), where an efficient technique of density functional perturbation theory (DFPT) is often applied to compute phonon frequencies. For anharmonic crystals (and also liquids), the molecular dynamics (MD) method is instead employed to calculate finite  $T$  elasticity (e.g., Kawai & Tsuchiya 2015). The DFPT + QHA for free energy are also applied to calculate high- $P, T$  thermodynamics and phase stabilities (e.g., Tsuchiya et al. 2004a,c).

### 3. STABILITY AND ELASTICITY OF MAJOR LOWER MANTLE PHASES

#### 3.1. Fe-Bearing $\text{MgSiO}_3$

In Earth’s lower mantle,  $(\text{Mg,Fe})\text{SiO}_3$  Br is considered the most abundant mineral, more than 60% in volume (e.g., Poirier 2000). It has the orthorhombically distorted perovskite structure with the space group  $Pbnm$  (Figure 1a). This crystal structure has in total  $10^\circ$  of freedom in the internal structural parameters including the three cell lengths. Besides, orthorhombic cells have nine independent elastic constants. For the computation of this kind of complicated crystal, the plane-wave basis and pseudopotential method are clearly the most practical technique even with high numerical accuracy. Those of pure  $\text{MgBr}$  were calculated within the density functional ab initio framework by Karki et al. (1997a) at static (0 K) conditions and by Wentzcovitch et al. (2004) at high  $T$  as a function of  $P$ . These studies indicate that the  $P$  dependences of the elastic wave velocities, both  $V_P$

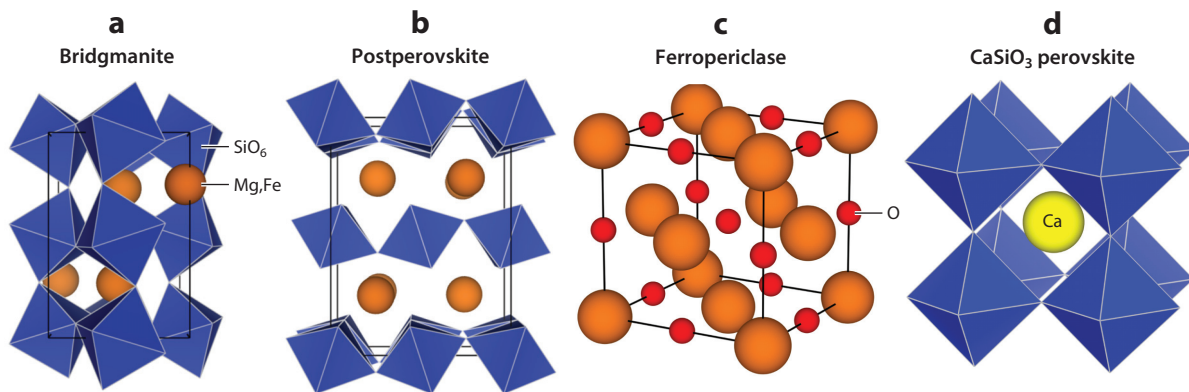
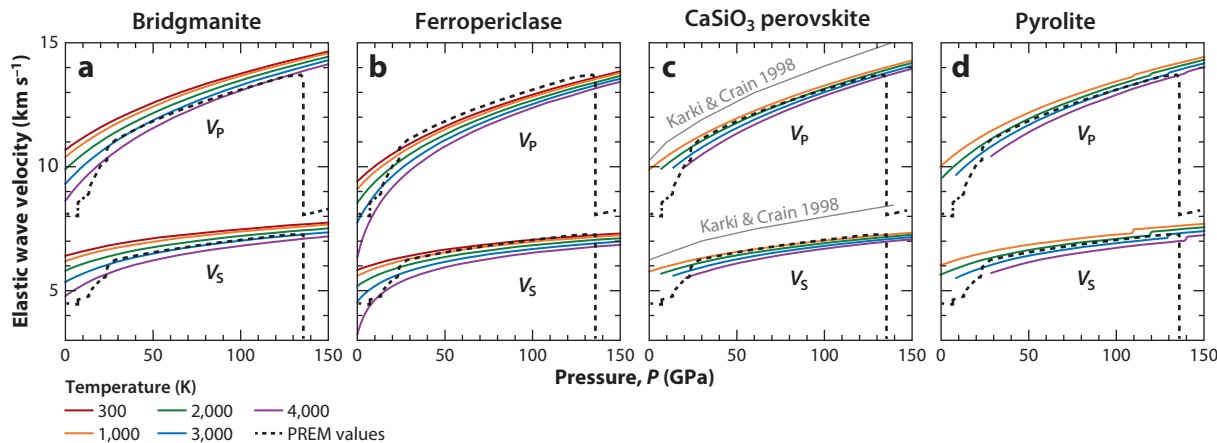


Figure 1

Crystal structures of the major lower mantle phases of (a) bridgmanite, (b) postperovskite, (c) ferropericlase, and (d)  $\text{CaSiO}_3$  perovskite.



**Figure 2**

Calculated elastic wave velocities of (a) bridgmanite (Br), (b) ferropericlasite (Fp), (c)  $\text{CaSiO}_3$  perovskite, and (d) pyrolitic aggregate with 6.25 mol%  $\text{Fe}^{3+}\text{Al}^{3+}\text{O}_3$  in Br and 12.5 mol%  $\text{Fe}^{2+}\text{O}$  in Fp as a function of pressure  $P$  at five values of temperature. Black dashed lines represent the Preliminary Reference Earth Model (PREM) values. Solid gray thin lines in panel c represent the velocities by Karki & Crain (1998). Kinks in panel d around 120 GPa correspond to the velocity jumps associated with the postperovskite transition.

and  $V_S$  of MgBr, match the Preliminary Reference Earth Model (PREM) (Dziewonski & Anderson 1981) in the lower mantle condition fairly well, which is supportive of the current generally accepted idea that this phase is the most dominant there.

A phase transition of Br was discovered at  $\sim 125$  GPa and  $\sim 2,500$  K (Murakami et al. 2004, Oganov & Ono 2004, Tsuchiya et al. 2004c) with  $\sim 0.5\%$  and  $\sim 2\%$  jumps in the P- and S-wave velocities, respectively (Tsuchiya et al. 2004b, Wentzcovitch et al. 2006). Since this  $P,T$  condition and these velocity jumps correspond closely to the depth and magnitude of so-called  $D''$  seismic discontinuity, this phase change has attracted considerable multidisciplinary interest over geophysics, mineral physics, and also materials science (e.g., Lay et al. 2005, Hirose 2006). The high- $P$  PPv phase is presently thought to be responsible, even in part, for several enigmatic properties observed in this region—from the core-mantle boundary (CMB) to  $\sim 300$  km above—such as lateral seismic wave velocity discontinuity, large heterogeneity, anisotropy, and thin ultralow seismic wave velocity zones atop the CMB. PPv has the  $\text{CaIrO}_3$ -type structure with space group  $Cmcm$  (Figure 1b) (Tsuchiya et al. 2004c). From the overall behavior of the elastic constants, of which specific values are reported elsewhere as a function of  $P$  (Tsuchiya et al. 2004b), it is clear that the structure is quite anisotropic and that anisotropy is strongly  $P$  dependent.

As is widely known, heavy iron decreases the acoustic wave speeds. Several studies investigated the effects of Fe and Al on the elasticity of Br and PPv based on the ab initio method (e.g., Caracas & Cohen 2005, Tsuchiya & Tsuchiya 2006, Stackhouse & Brodholt 2008) and indicated that elastic moduli of Br are less sensitive to iron, while it directly affects density. Calculated  $V_P$  and  $V_S$  of 6.25 mol%  $\text{Fe}^{2+}\text{SiO}_3$ -bearing Br are shown in Figure 2 as an example.

### 3.2. (Mg,Fe)O

The next major mineral phase in Earth's lower mantle after ferrosilicate Br,  $(\text{Mg}_{1-x}\text{Fe}_x)\text{SiO}_3$ , is believed to be  $(\text{Mg}_{1-x}\text{Fe}_x)\text{O}$  Fp (e.g., Poirier 2000). The magnesium end member of Fp, periclasite, possessing the B1 (NaCl) structure (Figure 1c) is known to be an extraordinarily stable phase. Although no structural phase transitions in this material have been observed or predicted under

the  $P,T$  conditions of the entire mantle, the spin state of  $\text{Fe}^{2+}$  in Fp is known to change from the high-spin (HS) to the low-spin (LS) state in the lower mantle  $P$  range (Badro et al. 2003, Lin et al. 2005, Tsuchiya et al. 2006b). This spin transition is an electronic transition caused by a change in the occupation manner of iron  $3d$  states and does not accompany any change in the crystal structure in the case of Fp. Nevertheless, some studies suggested anomalous softening of  $V_P$  of Fp across the spin transition and discussed its seismological visibility (e.g., Crowhurst et al. 2008, Marquardt et al. 2009a). This behavior is considered to be associated with an increase of compressibility within the spin transition  $P$  range (the mixed-spin state region). However, the mixed-spin state region is expected to become broader at higher  $T$  due to the mixing entropy effect of HS and LS irons (Tsuchiya et al. 2006b). The spin transition  $P$  of iron in Fp was reported to depend strongly on the iron configuration (Cheng et al. 2018), suggesting that the configurational disordering of iron in Fp also enhances the mixed-spin region. At the lower mantle  $T$ , the anomaly would therefore turn out to be smeared out even if it exists at low  $T$ . **Figure 2b** indicates  $V_P$  and  $V_S$  of Fp including 12.5 mol%  $\text{Fe}^{2+}\text{O}$  calculated combining internally consistent LDA +  $U$ , LD, and QHA.

Marquardt et al. (2009b) also pointed out that the spin crossover in Fp affects its elastic anisotropy. LS Fp was reported to have at least 50% stronger shear anisotropy in the lowermost mantle compared to  $\text{MgO}$ , which is originally even quite anisotropic at high  $P$  (Karki et al. 1999, Tsuchiya & Kawamura 2001, Wentzcovitch et al. 2006). In Fe-bearing Br with geophysically relevant Fe concentration (6.25%), an HS to LS transition occurs only for Fe replaced in the Si site, and the HS state remains stable when Fe is replaced in the Mg site even above 200 GPa (Wang et al. 2015). When Br possesses not only Fe but also Al as seen in the natural peridotitic and basaltic compositions, larger Fe ions and smaller Al ions are partitioned preferentially to the Mg and Si sites, respectively, so that the spin transition is less likely in Br.

### 3.3. $\text{CaSiO}_3$

$\text{CaSiO}_3$  perovskite (CaPv) is thought to be the third abundant phase in the lower mantle with the fraction up to 7–8 vol% (e.g., Irifune 1994). Despite its importance, there were some unanswered questions about the structure, stability, equation of state, and also elastic properties of CaPv under high  $P,T$ , which complicate some attempts to model the mineralogy of the lower mantle (Stacey & Isaak 2001).  $\text{CaSiO}_3$  crystallizes to the Pv structure over 10–13 GPa, depending on  $T$ , and is known to be unquenchable at ambient conditions. At lower mantle conditions,  $\text{CaSiO}_3$  has an ideal cubic Pv structure (space group  $Pm\bar{3}m$ ) (**Figure 1d**), while at lower  $T$  it was suggested to be slightly distorted (Stixrude et al. 1996, Magyari-Köpe et al. 2002, Shim et al. 2002, Caracas et al. 2005). While the small degree of the possible distortion is hardly observed by current high- $P,T$  X-ray techniques, Caracas et al. (2005) theoretically investigated the symmetrically related structural derivatives of  $\text{CaSiO}_3$  based on the vibrational property of the parent cubic phase. They examined nine modifications having different symmetries and reported that the tetragonal  $I4/mcm$  atomic configuration with out-phase rotations of  $\text{SiO}_6$  octahedra is the most stable at 0 K. The enthalpy difference between this  $I4/mcm$  and the cubic Pv phase increased with increasing  $P$ , indicating that the  $I4/mcm$  structure becomes more stable relative to the cubic structure at higher  $P$ .

Li et al. (2006), Stixrude et al. (2007), and Tsuchiya (2011) found that CaPv with the tetragonal distortion has distinctly smaller shear moduli than cubically constrained CaPv. As a result, cubically constrained CaPv yielded anomalously faster  $V_P$  and, in particular,  $V_S$  than tetragonal distorted CaPv, and Stixrude et al. (2007) suggested that significant velocity increases are expected to occur across the tetragonal-to-cubic transition at  $T$  near the mantle geotherm. This elasticity for cubic CaPv was, however, inappropriate because of insufficient structural relaxations (Tsuchiya 2011,

Kawai & Tsuchiya 2015). By allowing the out-phase octahedral rotations also when strains are applied to cubic CaPv, which can be achieved by taking a supercell the same as the tetragonal structure, the shear modulus became substantially smaller even in cubic CaPv. This resulted in producing significantly slower velocities for cubic CaPv, both in  $V_P$  and in  $V_S$  (**Figure 2c**), which are confirmed by a recent ultrasonic experiment (Gréaux et al. 2019) but at lower  $P, T$  only. Although Stixrude et al. (2007) suggested an elastic anomaly accompanied by the tetragonal-cubic phase change in CaPv, this in principle might be unlikely because this type of structural transition is associated with the zone boundary optic phonon instability, not with the zone center acoustic phonon instability (e.g., Gesi et al. 1972). Due to the vibrational instability of the cubic phase, the LD method cannot be applied to calculate its high- $P, T$  elasticity; instead, the MD method has to be used.

### 3.4. Aggregate Elasticity

Using the calculated elasticity of Fe-bearing Br and Fp, Wang et al. (2015) modeled the seismic wave velocities of some representative rock compositions, chondritic (Br:Fp  $\sim$  9:1 in volume), pyrolitic (8:2), and olivine (7:3), and reported that the pyrolitic aggregate matches the one-dimensional velocities of PREM best. Here we model the velocities of pyrolitic aggregate including the PPv and CaPv (**Figure 2d**). Due to the similarity in the P- and S-wave velocities of Fe-bearing Br and CaPv, a small fraction of CaPv in the pyrolitic composition has almost no effect on the aggregate elasticity. **Figure 2d** clearly shows this compositional model can reproduce the seismological lower mantle model at the reasonable  $T$  range (from  $\sim$ 1,900 to  $\sim$ 2,500 K), as reported in Wang et al. (2015). In this modeling, however, there exist tradeoffs between the Br/Fp ratio and geotherm if the Fe concentrations are treated as free parameters. Therefore, we fix them to petrological values (8 mol% in Br and 18 mol% in Fp) (Wang et al. 2015). Although these are representative ones measured experimentally, some fluctuations might be possible in the whole lower mantle. Uncertainties caused by  $\pm$ 1 mol% variations in the concentration of Fe were then examined, which correspond to the line width for the calculated velocities in **Figure 2d**. Elastic wave velocities of CaPv-bearing aggregates previously evaluated by using existing physical parameters and empirical relationships (Stixrude & Lithgow-Bertelloni 2005) are substantially overestimated, since those were evaluated based on the elasticity of CaPv by applying the incorrect structural relaxations (Sherman 1993, Karki & Crain 1998).

Pyrolite is the compositional model made to explain the upper mantle (Ringwood 1962). The ab initio elasticity suggests that pyrolite is also a good candidate for the major element chemistry of the lower mantle. This compositional similarity of the upper and lower mantles implies a global materials circulation in the whole mantle rather than separated convections in the shallower and deeper portions. This mineral physical view of Earth's mantle dynamics is consistent with recent seismic tomography models (e.g., Eberle et al. 2002, Zhao 2004, Takeuchi 2007, French & Romanowicz 2015), which image continuous flows between the shallow portion and the base of the mantle, and also with fluid dynamics simulations showing the global mantle convection (e.g., Nakagawa & Tackley 2011). Since the pyrolite composition has a smaller amount of SiO<sub>2</sub> than primitive chondrites, the pyrolitic mantle also requires the Si-bearing core if chondrites were the building blocks of Earth (Allègre et al. 1995).

### 3.5. Postperovskite Phase Relations in Fe- and Al-Bearing Systems

For realistic multicomponent systems such as the peridotitic, basaltic, and pyrolitic compositions, not only Fe but also Al<sub>2</sub>O<sub>3</sub> are substantially accommodated in Br (Irifune & Ringwood 1993,

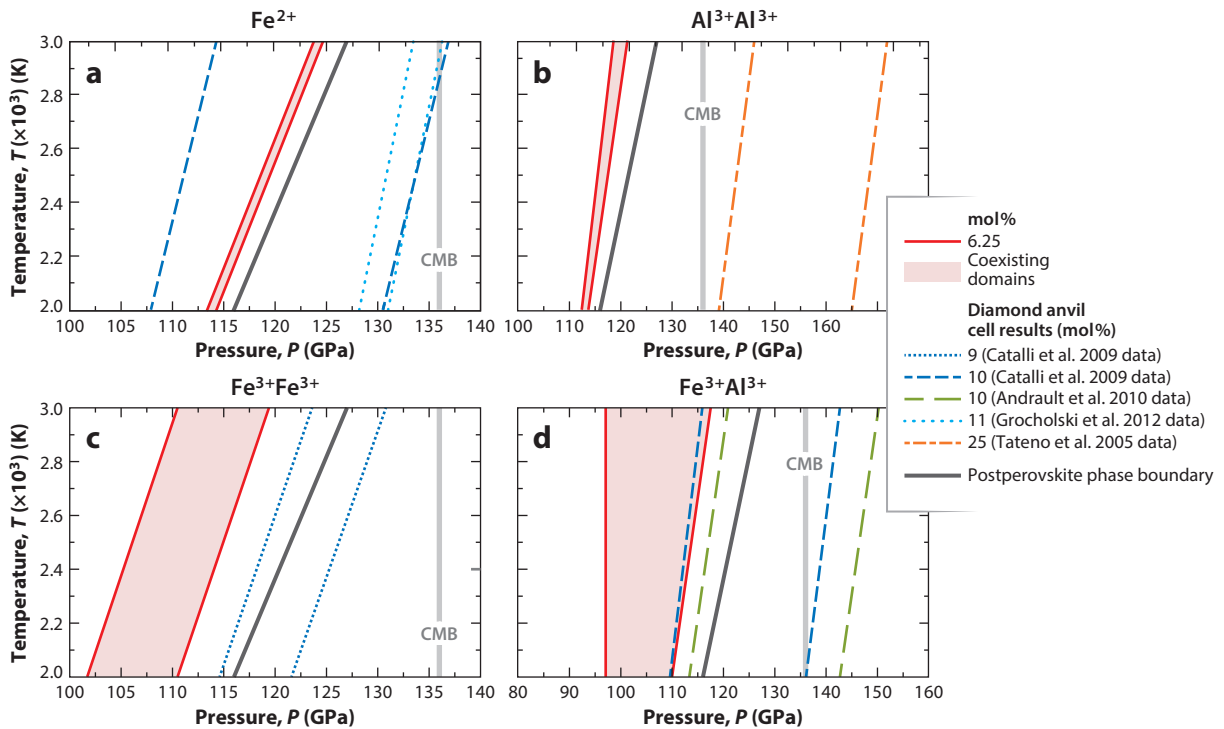


**Figure 3**

Postperovskite phase boundaries calculated for  $\text{Fe}^{2+}$ -,  $\text{Fe}^{3+}$ -, and/or  $\text{Al}^{3+}$ -bearing systems. Calculated two-phase coexisting domains are represented by red shaded areas. Dashed lines are the laser-heated diamond anvil cell results. Abbreviation: CMB, core-mantle boundary. Figure adapted from Wang et al. (2019).

Irifune 1994). Understanding the effects of these elements on the stability and elasticity of Br and PPv is therefore important. The solid solution of these elements in general produces two-phase coexisting domains. Since phase transitions occur gradually in the two-phase domains, narrow loop widths (typically less than  $\sim 80$  km) are in general necessary to interpret the sharp seismic discontinuity. Actually, recent ab initio simulations of finite  $T$  free energy in the  $\text{MgSiO}_3$ - $\text{Al}_2\text{O}_3$  system clarified a sufficiently small Br + PPv two-phase coexisting domain (Tsuchiya & Tsuchiya 2008, Wang et al. 2019) (**Figure 3**), where effects of the atomic random distribution were captured through the multiple configuration sampling technique. Similar calculations have been conducted for the phase relations in  $\text{MgSiO}_3$ - $\text{FeSiO}_3$  (or  $\text{Fe}_2\text{O}_3$ ), and it was reported that broad two-phase coexisting domains interestingly appear for the  $\text{Fe}^{3+}$ -bearing cases (Wang et al. 2019) (**Figure 3**). This implies that the places where the  $D''$  discontinuity is observed should not be highly oxidized. The reduced condition in the  $D''$  seems reasonable considering the proximity of the liquid iron core. Although some high- $P$  experiments reported considerably broad two-phase coexisting domains (Tateno et al. 2005, Catalli et al. 2009, Andrault et al. 2010, Grocholski et al. 2012), two-phase widths and even transition pressures themselves are quite different in different experiments, suggesting fundamental technical difficulty in accurate determination of multicomponent phase relations by using the laser-heated diamond anvil cell technique around 100 GPa. Also in ab initio computations, absolute  $P, T$  positions of the phase boundaries could change depending on the treatment of exchange and correlation potentials (e.g., LDA or GGA) by an  $\sim 10$  GPa maximum

as explained in Section 2; their relative differences such as the widths of two-phase loops are rather insensitive to it.

## 4. DENSE HYDROUS PHASES

### 4.1. Transportation of Water into the Deep Earth

The circulation of water in the deep Earth is believed to have important effects on the dynamics of the mantle, since experimental and theoretical studies have repeatedly reported that the physical properties of rocks and minerals are significantly altered by the coexistence of water. Hydrogen is the most abundant element in the universe and mainly exists as liquid water, the liquid phase of  $\text{H}_2\text{O}$ , on Earth's surface. It is transported into Earth's interior by hydrous minerals in the subducting slabs. Although most of the hydrous minerals decompose at depths shallower than 120 km, some hydrous minerals might be retained in the subducting cold ( $\sim 500$  K colder than the average mantle geotherm) slab without being completely dehydrated and transported to the greater depths. The seismic observations suggest that some of the subducting plate reaches the mantle transition zone, the lower mantle, and even the CMB (e.g., Eberle et al. 2002, Zhao 2004, Takeuchi 2007).

### 4.2. New Hydrous Minerals in the Lower Mantle

Hydrous minerals have long been believed to be destabilized under high pressure and to be impossible to exist in the deep lower mantle. However, this view has been drastically changed by recent ab initio computations and related experiments, and new models on the water circulation in Earth's interior have been proposed. Recent advancements and discoveries on new dense hydrous phases are reviewed in this section.

**4.2.1. Phase H.** When lower- $P$  hydrous silicates such as serpentine and phase A are transported to the upper part of the lower mantle with the subducting slab, superhydrous phase B [ $\text{Mg}_{10}\text{Si}_3\text{O}_{14}(\text{OH})_4$ ] is stabilized. At higher  $P$ , superhydrous phase B further transforms to phase D ( $\text{MgSi}_2\text{O}_6\text{H}_2$ ). Through these structure transitions, their layered structures change to three-dimensional network structures accommodating to a high- $P$  environment, increasing the cation coordination number from 4 to 6. Since hydrogen atoms have small X-ray scattering cross sections and can hardly be detected by X-ray diffraction experiments, the behavior of hydrogen in hydrous minerals under high  $P$  has not been sufficiently understood. The ab initio calculation method is therefore an effective means to investigate it.

Previously, it was reported that phase D decomposes to an anhydrous mineral and water at about 40 GPa or phase transition to an unknown phase (Shieh et al. 2000), and it was believed that the transport of water to the deep Earth by dense hydrous magnesium silicates (DHMSs) is terminated in the middle of the lower mantle at about 1,250 km depth (e.g., Albarède 2009). An ab initio study (Tsuchiya 2013), however, found that phase D might be dissociated into a new hydrous mineral ( $\text{MgSiO}_4\text{H}_2$ ) and stishovite ( $\text{SiO}_2$ ) at  $\sim 40$  GPa. Following this theoretical prediction, in situ synchrotron X-ray diffraction experiments were conducted at SPring-8 and revealed that phase D transforms into the same structure in the predicted  $P$  condition (Nishi et al. 2014). This new phase was identified as the highest- $P$  DHMS almost 30 years after the discovery of phase D and named phase H. This phase H has an  $\text{MgSiO}_4\text{H}_2$  composition, and the crystal structure is similar to the  $\text{CaCl}_2$ -type structure, which is isostructural to stishovite (a high- $P$  phase of  $\text{SiO}_2$ ) and  $\delta$ - $\text{AlOOH}$  (Tsuchiya et al. 2002) (**Figure 4**). This structure has a disordered Mg and Si arrangement in the unique octahedral site at the mantle  $T$  condition (Bindi et al. 2014, Tsuchiya & Mookherjee 2015).

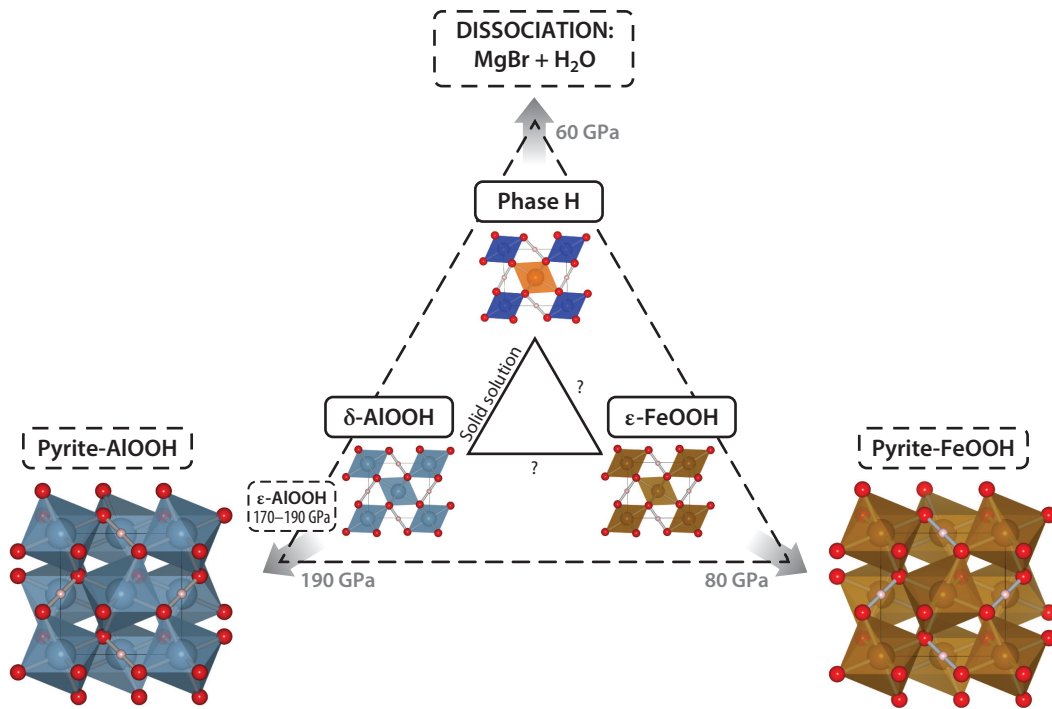


**Figure 4**

Crystal structures of phase H, dense AIOOH, and FeOOH and the schematic diagram of the  $\text{MgSiO}_4\text{H}_2$ -AIOOH-FeOOH ternary system under high pressure. Abbreviation: Br, bridgmanite.

Pristine phase H was clarified to have only a narrow stability field and decompose into MgBr with  $\text{H}_2\text{O}$  at 52 GPa, the mid-lower mantle  $P$  condition, and static 0 K (Tsuchiya 2013), which was confirmed by subsequent high- $P$  experiments (Ohtani et al. 2014). However, the actual mantle has complex chemistry with magnesium silicates plus several wt% of Al, Fe, and so on. It has been shown by high- $P$  experiments that Al is preferably partitioned to phase H in the multicomponent system, which significantly expands the stability region of phase H (Nishi et al. 2014, Ohira et al. 2014). The system can be approximated as a solid solution of phase H and  $\delta$ -AIOOH, which has the same crystal structure as phase H, and  $\delta$ -AIOOH is stable in a very wide  $P, T$  range (33–134 GPa, 1,350–2,300 K) (Sano et al. 2008a). It can therefore be expected that the Al incorporation enhances the stability of phase H down to the CMB region.

**4.2.2. Pyrite-type FeOOH.** It was theoretically predicted that  $\delta$ -AIOOH undergoes phase transition to a pyrite structure above 170 GPa (Tsuchiya & Tsuchiya 2011) via an intermediate  $\epsilon$ -phase (Verma et al. 2018). This structure was also confirmed theoretically and experimentally to be stable in GaOOH and InOOH compositions (Tsuchiya et al. 2008, Sano et al. 2008b). The pyrite-type structure is widely known to be stable in dioxides,  $\text{SiO}_2$  and  $\text{GeO}_2$  above 250 GPa and 90 GPa, respectively (Ono et al. 2003, Kuwayama et al. 2005). However, the  $\alpha$ - $\text{PbO}_2$ -type phase, an intermediate phase between  $\text{CaCl}_2$ -type and pyrite-type in  $\text{SiO}_2$  (seifertite), seems not to be stabilized in MOOH compositions ( $M = \text{Al, Ga, In}$ ).

As mentioned above, the solid solution of  $\delta$ -AlOOH and phase H is considered to have a very wide stability field. However, its density is notably smaller compared to anhydrous mantle rocks such as pyrolite, and thus the gravitational stability is questioned to be responsible for water transport to the deep Earth. Interestingly,  $\epsilon$ -FeOOH, the high- $P$  phase of  $\alpha$ -FeOOH (goethite), is also known to have the same structure as  $\delta$ -AlOOH. A transition from the HS to LS state was predicted in  $\epsilon$ -FeOOH at about 50 GPa with a volume reduction of  $\sim 10\%$ , resulting in stabilizing this hydrous phase considerably under high  $P$  (Gleason et al. 2013). More recent ab initio calculations of FeOOH showed a further high- $P$  phase transition to the pyrite-type structure at  $\sim 70$  GPa, and this new phase transition was successfully confirmed experimentally at  $\sim 80$  GPa (Nishi et al. 2017). It is surprising that this phase is stable even at average mantle  $T$  and has a significantly higher density than other hydrous minerals such as phases H and  $\delta$ -AlOOH, suggesting that the solid solution between phase H, AlOOH, and FeOOH would be deeply related to the gravitational stability of hydrous minerals in the deep Earth.

### 4.3. Insight into the Water Circulation in the Lower Mantle

Although phase H has a very low density compared to the anhydrous lower mantle minerals (thus it is not gravitationally stable), it was confirmed that the new FeOOH phase is both thermodynamically and gravitationally stable even in the deepest lower mantle region, suggesting a new possibility for the water transport down to the CMB. Considering that the thermodynamic stability of phase H is enhanced by the Al incorporation and FeOOH and AlOOH form a solid solution, DHMSs could become stable in the lower mantle even at normal geotherm by the incorporations of Al and Fe. Indeed, like aluminous phase H, superaluminous phase D ( $\text{Al}_2\text{SiO}_6\text{H}_2$ ) is also reported to be stable above 2,273 K at lower mantle  $P$  (Pamato et al. 2015). In both aluminous phase D and phase H, Al is incorporated by a coupled substitution mechanism ( $\text{Mg} + \text{Si} \leftrightarrow 2\text{Al}$ ). Mg atoms usually situate in the sixfold coordination sites in DHMSs, but the ionic radius of Mg is generally too large, resulting in destabilizing the structures. Incorporations of small Al and LS Fe into the Mg sites could help to suppress this structural disadvantage and to enhance the thermodynamic stability of DHMSs. A possibility of further water transport to the core through the core-mantle chemical interaction would be an interesting research topic to clarify the deep Earth global water circulation.

These recent findings evidenced the much wider  $P, T$  stabilities of hydrous minerals than previously thought. A recent mantle convection simulation considering those new stabilities reported that the present mantle possesses water 11 times larger in amount than the current surface ocean mass as maximum (Nakagawa et al. 2018). Water might change the physical properties of minerals and rocks in the lower mantle considerably. They have, however, not been sufficiently clarified yet. Specifically, water may change (a) melting temperature, (b) rheology (e.g., viscosity, yield strength, and deformation properties), and (c) phase relations of minerals. It has been reported that the melting temperature of hydrous FeOOH is lower than that of the surrounding mantle, and FeOOH presumably contributes to produce a partial melt at the lowermost mantle (Nishi et al. 2017, Deng et al. 2019). Such melt might explain the ultralow velocity zones seismologically observed at the CMB (e.g., Garnero & McNamara 2008). Regarding the rheology, an MD study has reported that the hydrolytic weakening in the lower mantle has a limited effect on the rheology (Muir & Brodholt 2018), whereas the elasticity of Br has been reported to be remarkably sensitive to the presence of hydrogen (Jiang & Zhang 2019). The clarification of the effects of water in the lower mantle should be an important subject in future studies. The actual presence of water in the lower mantle was supported by a discovery of natural diamond inclusions with fluid remnants (Palot et al. 2016), although its global distribution is still unrevealed.

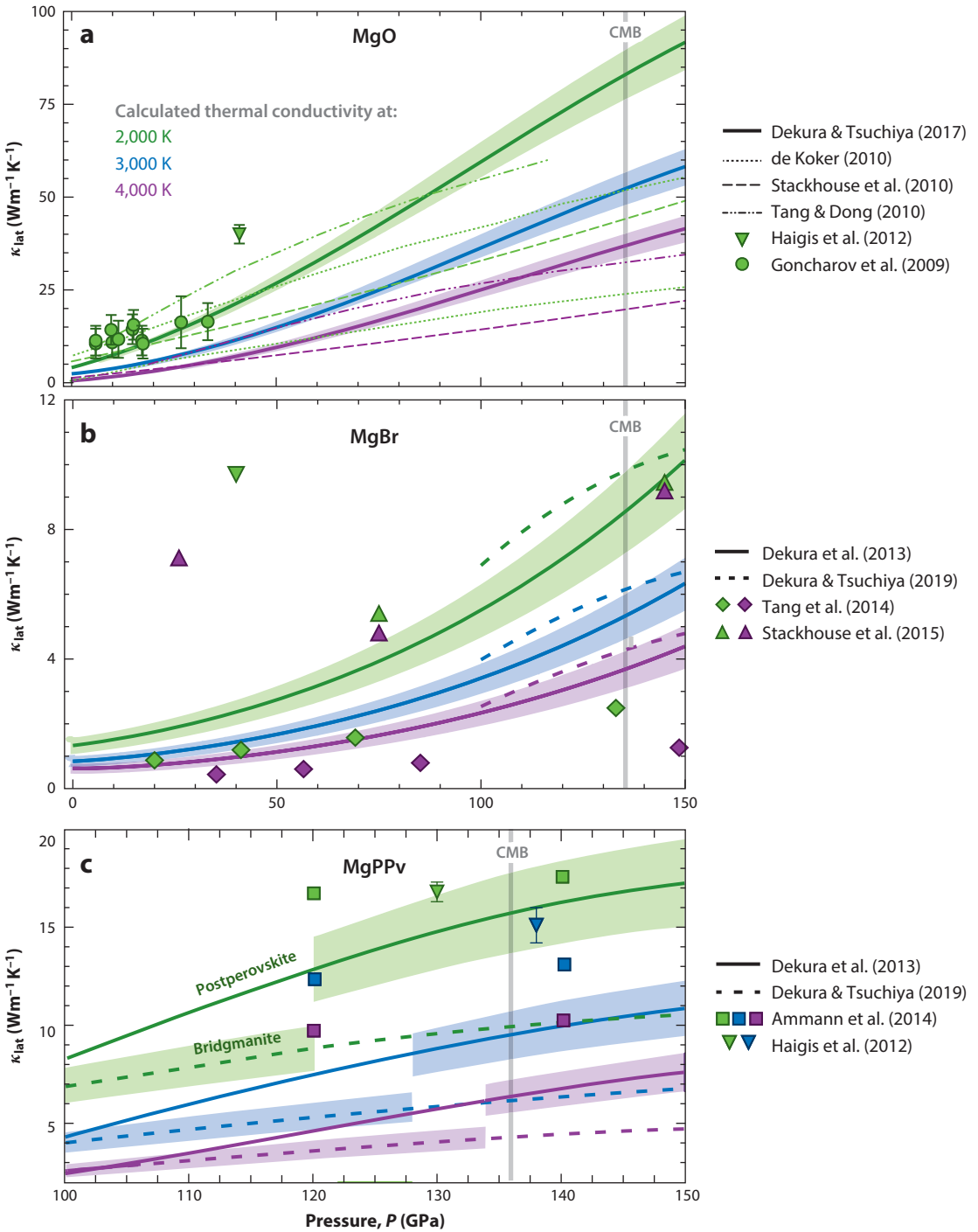
## 5. TRANSPORT PROPERTY

### 5.1. Lattice Thermal Conductivity of the Lower Mantle Phases

The lattice thermal conductivity,  $\kappa_{\text{lat}}$ , of Earth's constituent materials is an important physical parameter in controlling the heat budget of Earth. The determination of this is, therefore, key to understanding the dynamics and thermal evolution of Earth's interior. In particular, detailed information of thermal conductivity of the lower mantle minerals, such as MgO, MgBr, and PPv, is important for determining the heat flow across the CMB, which governs important roles in the deep Earth, such as the style of mantle convection, evolution of the inner core, and generation of the magnetic field (e.g., Gubbins 2007, Lay et al. 2008). Despite this importance, experimental measurements of thermal conductivity of Earth's lower mantle minerals at high  $P, T$  have been limited so far primarily due to technical difficulty. Therefore, extrapolations of the thermal conductivity measured at much lower  $P, T$  conditions than the actual Earth's deep mantle condition are often made to estimate the lower mantle conductivity (Osako & Ito 1991; Katsura 1997; Hofmeister 1999; Goncharov et al. 2009, 2014; Manthilake et al. 2011; Ohta et al. 2012, 2017; Imada et al. 2014; Hsieh et al. 2017, 2018; Okuda et al. 2017). Such large extrapolations, however, cause considerable uncertainty under high  $P, T$ . Theoretical studies are therefore also quite important.

Although theoretical treatment of thermal conductivity has also been technically difficult, in recent years, ab initio methods have been extended to thermal conductivity of lower mantle minerals successfully (Dekura et al. 2013; Dekura & Tsuchiya 2017, 2019). The heat transport in insulator is governed by phonon conduction. The phonon conduction obeys the phonon Boltzmann transport equation, which describes changes in the population of phonon modes due to the phonon-phonon interaction in the presence of the  $T$  gradient (Omini & Sparavigna 1996). The phonon-phonon interaction is then described based on the anharmonic LD theory (Srivastava 1990), where the treatment for atomic potential up to third-order expansion is usually enough at the lower mantle  $P$  even at the mantle  $T$ .

At low  $P$  ( $< 10$  GPa) and 300 K, the ab initio anharmonic LD results agreed well with those obtained in experiments using single crystals (Dalton et al. 2013), with nonequilibrium ab initio MD (Stackhouse et al. 2010), and anharmonic LD with the simple relaxation time approximation (Tang & Dong 2010). In contrast, large discrepancies are seen in the experiments of polycrystalline samples (Imada et al. 2014). At higher  $P$  and 300 K, the calculated results deviate from the experimental values for single crystals (Dalton et al. 2013). This might be due to phonon scattering by crystal imperfections in experiments using the diamond anvil cell (Srivastava 1990). **Figure 5a** shows calculated thermal conductivity of MgO based on the ab initio anharmonic LD simulations (Dekura & Tsuchiya 2017) alongside thermal conductivity obtained from more approximated methods above 2,000 K. The ab initio anharmonic LD values (Dekura & Tsuchiya 2017) fall in the range of available experimental data (Dalton et al. 2013), ab initio MD (de Koker 2010, Stackhouse et al. 2010), and anharmonic LD with the relaxation time approximation (Tang & Dong 2010) up to  $\sim 35$  GPa. However, at higher  $P$ , the discrepancies in calculated thermal conductivity become substantial. The classical MD simulation at 2,000 K (Haigis et al. 2012) yielded much higher conductivities, particularly at  $P \sim 130$  GPa, where the use of empirical potentials might have affected the results. At the CMB conditions ( $P = 136$  GPa and  $T = 3,800$  K), their thermal conductivity is close to that obtained within the relaxation time approximation with the isotopic correction reported by Tang & Dong (2010). However, the  $P$  dependence at high  $P, T$  reported by Dekura & Tsuchiya (2017) is completely different from that found in Tang & Dong (2010). Discrepancies between Dekura & Tsuchiya (2017) and previous calculations (de Koker 2010, Stackhouse et al. 2010, Tang & Dong 2010) might have originated in insufficient cell sizes or MD time steps in the earlier simulations.



(Caption appears on following page)

**Figure 5** (Figure appears on preceding page)

Calculated lattice thermal conductivity of (a) MgO, (b) MgBr, and (c) MgPPv as a function of  $P$  at 2,000 (green), 3,000 (blue), and 4,000 K (purple) with computational uncertainties (shaded bands). The experimental values for MgO at 2,000 K (data from Goncharov et al. 2009) are also indicated (green circles), while no experimental data are available for Br and PPv in the corresponding  $P, T$  range so far. Abbreviations: Br, bridgmanite; CMB, core-mantle boundary;  $\kappa$ , lattice thermal conductivity;  $P$ , pressure; PPv, postperovskite;  $T$ , temperature. Figure adapted from Dekura et al. (2013) and Dekura & Tsuchiya (2017, 2019).

Although computation of thermal conductivity of Br is much heavier than that of MgO because of its complicated crystal structure, several ab initio anharmonic LD studies have recently been conducted (Dekura et al. 2013, Tang et al. 2014, Ghaderi et al. 2017, Dekura & Tsuchiya 2019) in addition to classical MD (Haigis et al. 2012) and ab initio nonequilibrium MD simulations (Stackhouse et al. 2015). At low  $T$  of 300 K, the earliest ab initio study based on the DFPT with the relaxation time approximation and Klemens approximation by Dekura et al. (2013) showed the thermal conductivity increases with increasing  $P$ , and it is in close agreement with experimental values (Osako & Ito 1991, Ohta et al. 2012) except for multi-anvil data (Manthilake et al. 2011). **Figure 5b** summarizes reported thermal conductivity of Br over 2,000 K. Tang et al. (2014) also calculated thermal conductivity based on the anharmonic LD within the relaxation time approximation and showed substantially small  $P$  dependence. We identify no clear reasons for this discrepancy so far. A possible reason is in the numerical setup for calculations of anharmonic force constants. Thermal conductivity determined by the classical MD simulations (Haigis et al. 2012) is found to be close to the solution of the Boltzmann transport equation. The potential reason for the discrepancy between the ab initio studies using the anharmonic LD with full solution of the linearized phonon Boltzmann transport equation (Ghaderi et al. 2017, Dekura & Tsuchiya 2019) and high- $P$  experiments (Manthilake et al. 2011, Ohta et al. 2012) might be due to the phonon-grain boundary scattering. At high- $P, T$ , the results of thermal conductivity calculated by ab initio anharmonic LD and MD simulations are scattered. For example, DFPT with the Klemens approximation (Dekura et al. 2013) and anharmonic LD with full solution of the linearized phonon Boltzmann transport equation (Ghaderi et al. 2017, Dekura & Tsuchiya 2019) provide  $\kappa_{\text{lat}} \sim 4 - 5$  W/m K at  $\sim 140$  GPa and 4,000 K. In contrast, ab initio real-space anharmonic LD with relaxation time approximation (Tang et al. 2014) provides considerably small conductivity of  $\sim 1$  W/m K, and ab initio nonequilibrium MD (Stackhouse et al. 2015) provides large values ( $\sim 9$  W/m K). The former is caused by substantially small  $P$  dependence of thermal conductivity, and the latter is responsible for its significantly weak  $T$  dependence, which is considerably smaller than the common  $T^{-1}$  dependence. Stackhouse et al. (2015) called this weak  $T$  dependence saturation, which was speculated to occur due to a decrease in the phonon mean free path down to interatomic spacings. The thermally averaged mean free path of Br is, however, found to be  $\sim 65$  Å at  $\sim 130$  GPa and 4,000 K (Dekura & Tsuchiya 2019), much longer than the interatomic Si-O distances ( $\sim 1.7$  Å) at this condition and even the supercell size used in Stackhouse et al. (2015).

**Figure 5c** shows the thermal conductivity of PPv calculated based on the anharmonic LD with full solution of the linearized phonon Boltzmann transport equation (Dekura & Tsuchiya 2019), indicating that the thermal conductivity of PPv is substantially higher than that of Br by more than 50%. Therefore, the PPv phase transition would make a jump in conductivity in the lowermost mantle. The thermal conductivity of PPv calculated at  $T = 2,000$  K based on the anharmonic LD (Dekura & Tsuchiya 2019) is found to be in reasonable agreement with the studies using the classical MD simulations (Haigis et al. 2012, Ammann et al. 2014) at 2,000 K. However, the values of these MD studies deviate from ours at higher  $T$ . One possible reason for this deviation might again lie in the use of the empirical model potentials in the classical simulations. The use of interatomic model potentials would easily fail to capture the detailed anharmonic properties at extremely high  $P, T$ .

## 5.2. Heat Transfer Across the Core-Mantle Boundary

Heat flow from the core to the mantle across the CMB, the surface integration of the CMB heat flux ( $q_{\text{CMB}}$ ), is the key indicator to represent the strength of the thermal coupling between the core and the mantle, where  $q_{\text{CMB}}$  can be evaluated by Fourier's law for the heat conduction as  $q_{\text{CMB}} = -\kappa_{\text{lat}} \nabla T$ . Based on the ab initio thermal conductivity of MgO, Br, and PPv determined by Dekura & Tsuchiya (2017 and 2019), the effective lower mantle conductivity of a pyrolitic PPv and MgO aggregate (8:2 volume ratio) at the CMB condition ( $P = 136$  GPa and  $T = 3,800$  K) is found by the Hashin-Shtrikman scheme to be  $11.7 \text{ Wm}^{-1}\text{K}^{-1}$ , which is  $\sim 40\%$  larger than that of a Br and MgO aggregate of  $8.5 \text{ Wm}^{-1}\text{K}^{-1}$  (Dekura & Tsuchiya 2019). The  $q_{\text{CMB}}$  is estimated for the hotter ( $\nabla T \sim 1.4$  K/km) and colder geotherms ( $\nabla T \sim 18$  K/km) to be  $23.5$  and  $204.8 \text{ mWm}^{-2}$ , respectively, indicating a substantial lateral variation expected in the CMB heat flux. This variation is enhanced by considering the phase transition since PPv has larger conductivity. Using the value of average CMB heat flux  $q_{\text{av}} = (q_{\text{cold}} + q_{\text{hot}})/2 \sim 114 \text{ mWm}^{-2}$ , the net CMB heat flow is estimated to be  $\sim 17$  TW, which is  $\sim 23\%$  larger than the Br + MgO case ( $\sim 13$  TW) (Dekura & Tsuchiya 2019). These values are comparable to that estimated recently from the core conductivity ( $\sim 15$  TW) (e.g., Pozzo et al. 2012). However, thermal conductivity can be reduced by incorporation of impurity (particularly Fe and Al) due to the phonon-impurity scattering.

The effects of Fe and Al incorporations on thermal conductivity should be investigated. Low- $T$  experiments on Fe-bearing MgO and Fe- and Al-bearing Br have reported substantial reduction of thermal conductivity by Fe incorporation (Manthilake et al. 2011, Goncharov et al. 2014, Ohta et al. 2017, Hsieh et al. 2018). Reductions of thermal conductivity by Fe and Al incorporation into Br were also reported (Manthilake et al. 2011, Hsieh et al. 2017, Okuda et al. 2017). However, the reported values are highly scattered, and the experimental  $P, T$  range is still limited. There also exists no study on the effects of Fe and Al on the lattice thermal conductivity of PPv so far. But we here try estimating aggregate conductivity even roughly using the most recent experimental data, reductions in conductivity of MgO by  $\sim 80\%$  and of Br (PPv) by  $\sim 40\%$  for incorporations of  $\sim 19$  mol% of FeO (Ohta et al. 2017) and  $\sim 7$  mol% of FeSiO<sub>3</sub> (Hsieh et al. 2017), respectively. The lowermost mantle conductivity is then estimated to be  $\sim 4.4 \text{ Wm}^{-1}\text{K}^{-1}$  for the pyrolitic aggregate. This value is  $\sim 62\%$  smaller than that for the Fe-free systems and produces the net CMB heat flow of  $\sim 6.4$  TW. The estimated heat flow is larger than that required to sustain the geodynamo at the current magnitude ( $\sim 2$ – $3.5$  TW) and leads to a relatively old inner core age ( $\sim 2$ – $2.5$  Ga). However, this heat flow is more than  $\sim 50\%$  smaller than that estimated from the core with high thermal conductivity of iron ( $\sim 15$  TW) (e.g., Pozzo et al. 2012). The heat flows estimated from the mantle and from the core should in principle match at the CMB. Although the solid solution effects of iron should be confirmed theoretically, this discrepancy in the CMB heat flow could be reconciled by the thermally or chemically stratified layer at the top of the outer core observed seismologically (Helffrich & Kaneshima 2010) if some subadiabatic temperature gradient exists there.

## 5.3. Plasticity

Elastic anisotropy is observed seismologically in some places of Earth's mantle, in particular near the boundary layers such as the upper mantle, mantle transition zone, and D'' layer (e.g., Karato 2003). Preferred lattice orientation of polycrystalline aggregates created by plastic deformation under high shear stress in corner flows is thought to be a candidate for the origin of seismic anisotropy. Under high- $P, T$  and low-strain rate condition, pure climb creep (Nabarro 1967) and recovery-controlled dislocation creep are expected, and atomic diffusivity is a key physical parameter to model the plastic deformation (e.g., Weertman 1957). Some preliminary ab initio studies

on atomic diffusivity (e.g., Karki & Khanduja 2006, 2007; Ammann et al. 2009, 2010; Ritterbex et al. 2018) and mechanical shear strength (e.g., Carrez et al. 2007, 2009; Metsue & Tsuchiya 2013) of the lower mantle minerals have been conducted. Future extensions of the techniques to more realistic situations could make theoretical quantifications of the deformation mechanism and viscosity of Earth's lower mantle.

## DISCLOSURE STATEMENT

The authors are not aware of any affiliations, memberships, funding, or financial holdings that might be perceived as affecting the objectivity of this review.

## ACKNOWLEDGMENTS

T.T. thanks Y. Fukao for the opportunity of this contribution and C. Shiraishi for the careful check of the manuscript. This work was supported by MEXT KAKENHI grants JP15H05826 and JP15H05834.

## LITERATURE CITED

- Albarède F. 2009. Volatile accretion history of the terrestrial planets and dynamic implications. *Nature* 461:1227–33
- Allègre CJ, Poirier JP, Humler E, Hofmann AW. 1995. The chemical composition of the Earth. *Earth Planet. Sci. Lett.* 134:515–26
- Ammann MW, Brodholt JP, Dobson DP. 2009. DFT study of migration enthalpies in MgSiO<sub>3</sub> perovskite. *Phys. Chem. Miner.* 36:151–58
- Ammann MW, Brodholt JP, Wookey J, Dobson DP. 2010. First-principles constraints on diffusion in lower-mantle minerals and a weak D'' layer. *Nature* 465:462–65
- Ammann MW, Walker AM, Stackhouse S, Wookey J, Forte AM, et al. 2014. Variation of thermal conductivity and heat flux at the Earth's core mantle boundary. *Earth Planet. Sci. Lett.* 390:175–85
- Andraut D, Munõz M, Bolfan-Casanova N, Guignot N, Perrillat J-P, et al. 2010. Experimental evidence for perovskite and postperovskite coexistence throughout the whole D'' region. *Earth Planet. Sci. Lett.* 293:90–96
- Anisimov VI, Gunnarsson O. 1991. Density-functional calculation of effective Coulomb interactions in metals. *Phys. Rev. B* 43:7570–74
- Badro J, Fiquet G, Guyot F, Rueff J-P, Struzhkin VV, et al. 2003. Iron partitioning in Earth's mantle: toward a deep lower mantle discontinuity. *Science* 300:789–91
- Bagno P, Jepsen O, Gunnarsson O. 1989. Ground-state properties of third-row elements with nonlocal density functionals. *Phys. Rev. B* 40:1997–2000
- Baroni S, Giannozzi P, Testa A. 1987. Green's-function approach to linear response in solids. *Phys. Rev. Lett.* 58:1861–64
- Bindi L, Nishi M, Tsuchiya J, Irifune T. 2014. Crystal chemistry of dense hydrous magnesium silicates: the structure of phase H, MgSiH<sub>2</sub>O<sub>4</sub>, synthesized at 45 GPa and 1000°C. *Am. Mineral.* 99:1802–5
- Caracas R, Cohen RE. 2005. Effect of chemistry on the stability and elasticity of the perovskite and post-perovskite phases in the MgSiO<sub>3</sub>-FeSiO<sub>3</sub>-Al<sub>2</sub>O<sub>3</sub> system and implications for the lowermost mantle. *Geophys. Res. Lett.* 32:L16310
- Caracas R, Wentzcovitch R, Price GD, Brodholt J. 2005. CaSiO<sub>3</sub> perovskite at lower mantle pressures. *Geophys. Res. Lett.* 32:L06306
- Carrez P, Ferré D, Cordier P. 2007. Peierls–Nabarro model for dislocations in MgSiO<sub>3</sub> post-perovskite calculated at 120 GPa from first principles. *Philos. Mag.* 87:3229–47
- Carrez P, Ferré D, Cordier P. 2009. Peierls–Nabarro modelling of dislocations in MgO from ambient pressure to 100 GPa. *Model. Simul. Mater. Sci. Eng.* 17:035010

- Catalli K, Shim SH, Prakapenka VB. 2009. Thickness and Clapeyron slope of the post-perovskite boundary. *Nature* 462:782–85
- Ceperley DM, Alder BJ. 1980. Ground state of the electron gas by a stochastic method. *Phys. Rev. Lett.* 45:566–69
- Cheng Y, Wang X, Zhang J, Yang K, Zhang C, et al. 2018. Investigation of iron spin crossover pressure in Fe-bearing MgO using hybrid functional. *J. Phys. Condens. Matter* 30:155403
- Cococcioni M, de Gironcoli S. 2005. Linear response approach to the calculation of the effective interaction parameters in the LDA + U method. *Phys. Rev. B* 71:035105
- Crowhurst JC, Brown JM, Goncharov AF, Jacobsen SD. 2008. Elasticity of (Mg,Fe)O through the spin transition of iron in the lower mantle. *Science* 319:451–53
- Dalton DA, Hsieh WP, Hohensee GT, Cahill DG, Goncharov AF. 2013. Effect of mass disorder on the lattice thermal conductivity of MgO periclase under pressure. *Sci. Rep.* 3:2400
- de Koker N. 2010. Thermal conductivity of MgO periclase at high pressure: implications for the D'' region. *Earth Planet. Sci. Lett.* 292:392–98
- Dekura H, Tsuchiya T. 2017. Ab initio lattice thermal conductivity of MgO from a complete solution of the linearized Boltzmann transport equation. *Phys. Rev. B* 95:184303
- Dekura H, Tsuchiya T. 2019. Lattice thermal conductivity of MgSiO<sub>3</sub> postperovskite under the lowermost mantle conditions from ab initio anharmonic lattice dynamics. *Geophys. Res. Lett.* 46:12919–26
- Dekura H, Tsuchiya T, Kuwayama Y, Tsuchiya J. 2011. Theoretical and experimental evidence for a new post-cotunnite phase of titanium dioxide with significant optical absorption. *Phys. Rev. Lett.* 107:045701
- Dekura H, Tsuchiya T, Tsuchiya J. 2013. Ab initio lattice thermal conductivity of MgSiO<sub>3</sub> perovskite as found in Earth's lower mantle. *Phys. Rev. Lett.* 110:025904
- Demuth T, Jeanvoine Y, Hafner J, Ángyán JG. 1999. Polymorphism in silica studied in the local density and generalized-gradient approximations. *J. Phys. Condens. Matter* 11:3833–74
- Deng J, Karki BB, Ghosh DB, Lee KKM. 2019. First-principles study of FeO<sub>2</sub>H<sub>x</sub> solid and melt system at high pressures: implications for ultralow-velocity zones. *J. Geophys. Res. Solid Earth* 124:4566–75
- Dziewonski AM, Anderson DL. 1981. Preliminary reference Earth model. *Phys. Earth Planet. Inter.* 25:297–356
- Eberle MA, Grasset O, Sotin C. 2002. A numerical study of the interaction between the mantle wedge, subducting slab, and overriding plate. *Phys. Earth Planet. Inter.* 134:191–202
- French SW, Romanowicz B. 2015. Broad plumes rooted at the base of the Earth's mantle beneath major hotspots. *Nature* 525:95–99
- Garnero EJ, McNamara AK. 2008. Structure and dynamics of Earth's lower mantle. *Science* 320:626–28
- Gesi K, Axe JD, Shirane G, Linz A. 1972. Dispersion and damping of soft zone-boundary phonons in KMnF<sub>3</sub>. *Phys. Rev. B* 5:1933–41
- Ghaderi N, Zhang DB, Zhang H, Xian J, Wentzcovitch RM, Sun T. 2017. Lattice thermal conductivity of MgSiO<sub>3</sub> perovskite from first principles. *Sci. Rep.* 7:5417
- Gleason AE, Quiroga CE, Suzuki A, Pentcheva R, Mao WL. 2013. Symmetrization driven spin transition in ε-FeOOH at high pressure. *Earth Planet. Sci. Lett.* 379:49–55
- Goncharov AF, Beck P, Struzhkin VV, Haugen BD, Jacobsen SD. 2009. Thermal conductivity of lower-mantle minerals. *Phys. Earth Planet. Int.* 174:24–32
- Goncharov AF, Lobanov SS, Tan X, Hohensee GT, Cahill DG, et al. 2014. Experimental study of thermal conductivity at high pressures: implications for the deep Earth interior. *Phys. Earth Planet. Int.* 247:11–16
- Gréaux S, Irifune T, Higo Y, Tange Y, Arimoto T, et al. 2019. Sound velocity of CaSiO<sub>3</sub> perovskite suggests the presence of basaltic crust in the Earth's lower mantle. *Nature* 565:218–21
- Grocholski B, Catalli K, Shim S, Prakapenka V. 2012. Mineralogical effects on the detectability of the post-perovskite boundary. *PNAS* 109:2275–79
- Gubbins D. 2007. Geomagnetic constraints on stratification at the top of Earth's core. *Earth Planets Space* 59:661–64
- Haigis V, Salanne M, Jahn S. 2012. Thermal conductivity of MgO, MgSiO<sub>3</sub> perovskite and post-perovskite in the Earth's deep mantle. *Earth Planet. Sci. Lett.* 355–356:102–8
- Hamann DR. 1996. Generalized gradient theory for silica phase transition. *Phys. Rev. Lett.* 76:660–63
- Hamann DR. 1997. H<sub>2</sub>O hydrogen bonding in density-functional theory. *Phys. Rev. B* 55:R10157–60

- Hashin Z, Shtrikman S. 1962. A variational approach to the theory of the elastic behaviour of polycrystals. *J. Mech. Phys. Solids* 10:343–52
- Helffrich G, Kaneshima S. 2010. Outer-core compositional stratification from observed core wave speed profiles. *Nature* 468:807–10
- Hill R. 1952. The elastic behaviour of a crystalline aggregate. *Proc. Phys. Soc. A* 65:349
- Hirose K. 2006. Postperovskite phase transition and its geophysical implications. *Rev. Geophys.* 44:RG3001
- Hofmeister AM. 1999. Mantle values of thermal conductivity and the geotherm from phonon lifetimes. *Science* 283:1699–706
- Hohenberg P, Kohn W. 1964. Inhomogeneous electron gas. *Phys. Rev. B* 136:864–71
- Hsieh WP, Deschamps F, Okuchi T, Lin JF. 2017. Reduced lattice thermal conductivity of Fe-bearing bridgmanite in Earth's deep mantle. *J. Geophys. Res. Solid Earth* 122:4900–17
- Hsieh WP, Deschamps F, Okuchi T, Lin JF. 2018. Effects of iron on the lattice thermal conductivity of Earth's deep mantle and implications for mantle dynamics. *PNAS* 115:4099–104
- Imada S, Ohta K, Yagi T, Hirose K, Yoshida H, Nagahara H. 2014. Measurements of lattice thermal conductivity of MgO to core-mantle boundary pressures. *Geophys. Res. Lett.* 41:4542–47
- Irfune T. 1994. Absence of an aluminous phase in the upper part of the Earth's lower mantle. *Nature* 370:131–33
- Irfune T, Ringwood AE. 1993. Phase transformations in subducted oceanic crust and buoyancy relationships at depths of 600–800 km in the mantle. *Earth Planet. Sci. Lett.* 117:101–10
- Jiang J, Zhang F. 2019. Theoretical studies on the hydrous lower mantle and D'' layer minerals. *Earth Planet. Sci. Lett.* 525:115753
- Karato S. 2003. *The Dynamic Structure of the Deep Earth: An Interdisciplinary Approach*. Princeton, NJ: Princeton Univ. Press
- Karki BB, Crain J. 1998. First-principles determination of elastic properties of CaSiO<sub>3</sub> perovskite at lower mantle pressures. *Geophys. Res. Lett.* 25:2741–44
- Karki BB, Khanduja G. 2006. Vacancy defects in MgO at high pressure. *Am. Mineral.* 91:511–16
- Karki BB, Khanduja G. 2007. A computational study of ionic vacancies and diffusion in MgSiO<sub>3</sub> perovskite and post-perovskite. *Earth Planet. Sci. Lett.* 260:201–11
- Karki BB, Stixrude L, Clark SJ, Warren MC, Ackland GJ, Crain J. 1997a. Structure and elasticity of MgO at high pressure. *Am. Mineral.* 82:51–60
- Karki BB, Stixrude L, Clark SJ, Warren MC, Ackland GJ, Crain J. 1997b. Elastic properties of orthorhombic MgSiO<sub>3</sub> perovskite at lower mantle pressures. *Am. Mineral.* 82:635–38
- Karki BB, Stixrude L, Crain J. 1997c. *Ab initio* elasticity of three high-pressure polymorphs of silica. *Geophys. Res. Lett.* 24:3269–72
- Karki BB, Wentzcovitch RM, de Gironcoli S, Baroni S. 1999. First-principles determination of elastic anisotropy and wave velocities of MgO at lower mantle conditions. *Science* 286:1705–7
- Katsura T. 1997. Thermal diffusivity of periclase at high temperatures and high pressures. *Phys. Earth Planet. Int.* 101:73–77
- Kawai K, Tsuchiya T. 2015. Small shear modulus of cubic CaSiO<sub>3</sub> perovskite. *Geophys. Res. Lett.* 42:2718–26
- Kohn W, Sham LJ. 1965. Self-consistent equations including exchange and correlation effects. *Phys. Rev. A* 140:1133–38
- Kuwayama Y, Hirose K, Sata N, Ohishi Y. 2005. The pyrite-type high-pressure form of silica. *Science* 309:923–25
- Lay T, Heinz D, Ishii M, Shim S-H, Tsuchiya J, et al. 2005. Multidisciplinary impact of the deep mantle phase transition in perovskite structure. *Eos Trans. AGU* 86:1–5
- Lay T, Hernlund J, Buffett BA. 2008. Core-mantle boundary heat flow. *Nat. Geosci.* 1:25–32
- Li L, Weidner DJ, Brodholt J, Alfè D, Price GD, et al. 2006. Elasticity of CaSiO<sub>3</sub> perovskite at high pressure and high temperature. *Phys. Earth Planet. Inter.* 155:249–59
- Lin J-F, Struzhkin VV, Jacobsen SD, Hu MY, Chow P, et al. 2005. Spin transition of iron in magnesiowüstite in the Earth's lower mantle. *Nature* 436:377–80
- Magyari-Köpe B, Vitos L, Grimvall G, Johansson B, Kollár J. 2002. Low-temperature crystal structure of CaSiO<sub>3</sub> perovskite: an *ab initio* total energy study. *Phys. Rev. B* 65:193107–11

- Manthilake GM, de Koker N, Frost DJ, McCammon CA. 2011. Lattice thermal conductivity of lower mantle minerals and heat flux from Earth's core. *PNAS* 108:17901–4
- Marquardt H, Speziale S, Reichmann HJ, Frost DJ, Schilling FR. 2009a. Single-crystal elasticity of  $(\text{Mg}_{0.9}\text{Fe}_{0.1})\text{O}$  to 81 GPa. *Earth Planet. Sci. Lett.* 287:345–52
- Marquardt H, Speziale S, Reichmann HJ, Frost DJ, Schilling FR, Garnero EJ. 2009b. Elastic shear anisotropy of ferropervicite in Earth's lower mantle. *Science* 324:224–26
- Metsue A, Tsuchiya T. 2011. Lattice dynamics and thermodynamic properties of  $(\text{Mg},\text{Fe}^{2+})\text{SiO}_3$  postperovskite. *J. Geophys. Res.* 116(B8):B08207
- Metsue A, Tsuchiya T. 2012. Thermodynamic properties of  $(\text{Mg},\text{Fe}^{2+})\text{SiO}_3$  perovskite at the lower mantle pressures and temperatures: an internally consistent LSDA+*U* study. *Geophys. J. Int.* 190:310–22
- Metsue A, Tsuchiya T. 2013. Shear response of Fe-bearing  $\text{MgSiO}_3$  post-perovskite at lower mantle pressures. *Proc. Jpn. Acad. B* 89:51–58
- Muir JMR, Brodholt JP. 2018. Water distribution in the lower mantle: implications for hydrolytic weakening. *Earth Planet. Sci. Lett.* 484:363–69
- Murakami M, Hirose K, Kawamura K, Sata N, Ohishi Y. 2004. Post-perovskite phase transition in  $\text{MgSiO}_3$ . *Science* 304:855–58
- Nabarro FRN. 1967. Steady-state diffusional creep. *Philos. Mag. A* 16:231–37
- Nakagawa T, Iwamori H, Yanagi R, Nakao A. 2018. On the evolution of the water ocean in the plate-mantle system. *Prog. Earth Planet. Sci.* 5:51
- Nakagawa T, Tackley PJ. 2011. Effects of low-viscosity post-perovskite on thermo-chemical mantle convection in a 3-D spherical shell. *Geophys. Res. Lett.* 38:L04309
- Nastar M, Willaime F. 1995. Tight-binding calculation of the elastic constants of fcc and hcp transition metals. *Phys. Rev. B* 51:6896–907
- Nishi M, Irifune T, Tsuchiya J, Tange Y, Nishihara Y, et al. 2014. Stability of hydrous silicate at high pressures and water transport to the deep lower mantle. *Nat. Geosci.* 7:224–27
- Nishi M, Kuwayama Y, Tsuchiya J, Tsuchiya T. 2017. The pyrite-type high-pressure form of  $\text{FeOOH}$ . *Nature* 547:205–8
- Oganov AR, Ono S. 2004. Theoretical and experimental evidence for a post-perovskite phase of  $\text{MgSiO}_3$  in Earth's  $D''$  layer. *Nature* 430:445–48
- Ohira I, Ohtani E, Sakai T, Miyahara M, Hirao N, et al. 2014. Stability of a hydrous  $\delta$ -phase,  $\text{AlOOH-MgSiO}_2(\text{OH})_2$ , and a mechanism of water transport into the base of lower mantle. *Earth Planet. Sci. Lett.* 401:12–17
- Ohta K, Yagi T, Hirose K, Ohishi Y. 2017. Thermal conductivity of ferropervicite in the Earth's lower mantle. *Earth Planet. Sci. Lett.* 465:29–37
- Ohta K, Yagi T, Taketoshi N, Hirose K, Komabayashi T, et al. 2012. Lattice thermal conductivity of  $\text{MgSiO}_3$  perovskite and post-perovskite at the core–mantle boundary. *Earth Planet. Sci. Lett.* 349–350:109–15
- Ohtani E, Amaike Y, Kamada S, Sakamaki T, Hirao N. 2014. Stability of hydrous phase  $\text{H MgSiO}_4\text{H}_2$  under lower mantle conditions. *Geophys. Res. Lett.* 41:8283–87
- Okuda Y, Ohta K, Yagi T, Sinmyo R, Wakamatsu T, et al. 2017. The effect of iron and aluminum incorporation on lattice thermal conductivity of bridgmanite at the Earth's lower mantle. *Earth Planet. Sci. Lett.* 474:25–31
- Omini M, Sparavigna A. 1996. Beyond the isotropic-model approximation in the theory of thermal conductivity. *Phys. Rev. B* 53:9064–73
- Ono S, Tsuchiya T, Hirose K, Ohishi Y. 2003. High-pressure form of pyrite-type germanium dioxide. *Phys. Rev. B* 68:014103
- Osako M, Ito E. 1991. Thermal diffusivity of  $\text{MgSiO}_3$  perovskite. *Geophys. Res. Lett.* 18:239–42
- Palot M, Jacobsen SD, Townsend JP, Nestola F, Marquardt K, et al. 2016. Evidence for  $\text{H}_2\text{O}$ -bearing fluids in the lower mantle from diamond inclusion. *Lithos* 265:237–43
- Pamato MG, Myhill R, Boffa-Ballaran T, Frost DJ, Heidelbach F, Miyajima N. 2015. Lower-mantle water reservoir implied by the extreme stability of a hydrous aluminosilicate. *Nat. Geosci.* 8:75–79
- Perdew JP, Burke K, Ernzerhof M. 1996. Generalized gradient approximation made simple. *Phys. Rev. Lett.* 77:3865–68

- Perdew JP, Chevary JA, Vosko SH, Jackson KA, Pederson MR, et al. 1992. Atoms, molecules, solids, and surfaces: applications of the generalized gradient approximation for exchange and correlation. *Phys. Rev. B* 46:6671–87
- Perdew JP, Zunger A. 1981. Self-interaction correction to density-functional approximations for many-electron systems. *Phys. Rev. B* 23:5048–79
- Poirier J-P. 2000. *Introduction to the Physics of the Earth's Interior*. Cambridge, UK: Cambridge Univ. Press
- Pozzo M, Davies C, Gubbins D, Alfè D. 2012. Thermal and electrical conductivity of iron at Earth's core conditions. *Nature* 485:355–58
- Ringwood AE. 1962. A model for the upper mantle. *J. Geophys. Res.* 67:857–67
- Ritterbex S, Harada T, Tsuchiya T. 2018. Vacancies in MgO at ultrahigh pressure: about mantle rheology of super-Earths. *Icarus* 305:350–57
- Sano A, Ohtani E, Kondo T, Hirao N, Sakai T, et al. 2008a. Aluminous hydrous mineral  $\delta$ -AlOOH as a carrier of hydrogen into the core–mantle boundary. *Geophys. Res. Lett.* 35:L03303
- Sano A, Yagi T, Okada T, Gotou H, Ohtani E, et al. 2008b. X-ray diffraction study of high pressure transition in InOOH. *J. Mineral. Petrol. Sci.* 103:152–55
- Sherman DM. 1993. Equation of state, elastic properties, and stability of CaSiO<sub>3</sub> perovskite: first principles (periodic Hartree-Fock) results. *J. Geophys. Res.* 98(B11):19795–805
- Shieh SR, Mao H-K, Hemley RJ, Ming LC. 2000. In situ X-ray diffraction studies of dense hydrous magnesium silicates at mantle conditions. *Earth Planet. Sci. Lett.* 177:69–80
- Shim S-H, Jeanloz R, Duffy TS. 2002. Tetragonal structure of CaSiO<sub>3</sub> perovskite above 20 GPa. *Geophys. Res. Lett.* 29:2166
- Srivastava GP. 1990. *The Physics of Phonons*. New York: Taylor & Francis
- Stacey FD, Isaak DG. 2001. Compositional constraints on the equation of state and thermal properties of the lower mantle. *Geophys. J. Int.* 146:143–54
- Stackhouse S, Brodholt JP. 2008. Elastic properties of the post-perovskite phase of Fe<sub>2</sub>O<sub>3</sub> and implications for ultra-low velocity zones. *Phys. Earth Planet. Inter.* 170:260–66
- Stackhouse S, Stixrude L, Karki BB. 2010. Thermal conductivity of periclase (MgO) from first principles. *Phys. Rev. Lett.* 104:208501
- Stackhouse S, Stixrude L, Karki BB. 2015. First-principles calculations of the lattice thermal conductivity of the lower mantle. *Earth Planet. Sci. Lett.* 427:11–17
- Stixrude L, Cohen RE, Yu R, Krakauer H. 1996. Prediction of phase transition in CaSiO<sub>3</sub> perovskite and implications for lower mantle structure. *Am. Mineral.* 81:1293–96
- Stixrude L, Lithgow-Bertelloni C. 2005. Thermodynamics of mantle minerals: 1. Physical properties. *Geophys. J. Int.* 162:610–32
- Stixrude L, Lithgow-Bertelloni C, Kiefer B, Fumagalli P. 2007. Phase stability and shear softening in CaSiO<sub>3</sub> perovskite at high pressure. *Phys. Rev. B* 75:024108
- Takeuchi N. 2007. Whole mantle SH velocity model constrained by waveform inversion based on three-dimensional Born kernels. *Geophys. J. Int.* 169:1153–63
- Tang X, Dong J. 2010. Lattice thermal conductivity of MgO at conditions of Earth's interior. *PNAS* 107:4539–43
- Tang X, Ntam MC, Dong J, Rainey ESG, Kavner A. 2014. The thermal conductivity of Earth's lower mantle. *Geophys. Res. Lett.* 41:2746–52
- Tateno S, Hirose K, Sata N, Ohishi Y. 2005. Phase relations in Mg<sub>3</sub>Al<sub>2</sub>Si<sub>3</sub>O<sub>12</sub> to 180 GPa: effect of Al on postperovskite phase transition. *Geophys. Res. Lett.* 32:L15306
- Tsuchiya J. 2013. First principles prediction of a new high-pressure phase of dense hydrous magnesium silicates in the lower mantle. *Geophys. Res. Lett.* 40:4570–73
- Tsuchiya J, Mookherjee M. 2015. Crystal structure, equation of state, and elasticity of phase H (MgSiO<sub>4</sub>H<sub>2</sub>) at Earth's lower mantle pressures. *Sci. Rep.* 5:15534
- Tsuchiya J, Tsuchiya T. 2008. Postperovskite phase equilibria in the MgSiO<sub>3</sub>-Al<sub>2</sub>O<sub>3</sub> system. *PNAS* 105:19160–64
- Tsuchiya J, Tsuchiya T. 2011. First-principles prediction of a high-pressure hydrous phase of AlOOH. *Phys. Rev. B* 83:054115

- Tsuchiya J, Tsuchiya T, Sano A, Ohtani E. 2008. First principles prediction of new high-pressure phase of InOOH. *J. Mineral. Petrol. Sci.* 103:116–20
- Tsuchiya J, Tsuchiya T, Tsuneyuki S. 2005. First principles study of hydrogen bond symmetrization of phase D under high pressure. *Am. Mineral.* 90:44–49
- Tsuchiya J, Tsuchiya T, Tsuneyuki S, Yamanaka T. 2002. First principles calculation of a high-pressure hydrous phase,  $\delta$ -AlOOH. *Geophys. Res. Lett.* 29:1909
- Tsuchiya T. 2011. Elasticity of subducted basaltic crust at the lower mantle pressures: insights on the nature of deep mantle heterogeneity. *Phys. Earth Planet. Inter.* 188:142–49
- Tsuchiya T, Caracas R, Tsuchiya J. 2004a. First principles determination of the phase boundaries of high-pressure polymorphs of silica. *Geophys. Res. Lett.* 31:L11610
- Tsuchiya T, Kawamura K. 2001. Systematics of elasticity: ab initio study in B1-type alkaline earth oxides. *J. Chem. Phys.* 114:10086–93
- Tsuchiya T, Tsuchiya J. 2006. Effect of impurity on the elasticity of perovskite and postperovskite: velocity contrast across the postperovskite transition in  $(\text{Mg,Fe,Al})(\text{Si,Al})\text{O}_3$ . *Geophys. Res. Lett.* 33:L12S04
- Tsuchiya T, Tsuchiya J, Umemoto K, Wentzcovitch RM. 2004b. Elasticity of post-perovskite  $\text{MgSiO}_3$ . *Geophys. Res. Lett.* 31:L14603
- Tsuchiya T, Tsuchiya J, Umemoto K, Wentzcovitch RM. 2004c. Phase transition in  $\text{MgSiO}_3$  perovskite in the Earth's lower mantle. *Earth Planet. Sci. Lett.* 224:241–48
- Tsuchiya T, Wang X. 2013. Ab initio investigation on the high-temperature thermodynamic properties of  $\text{Fe}^{3+}$ -bearing  $\text{MgSiO}_3$  perovskite. *J. Geophys. Res. Solid Earth* 118:83–91
- Tsuchiya T, Wentzcovitch RM, da Silva CRS, de Gironcoli S, Tsuchiya J. 2006a. Pressure induced high spin to low spin transition in magnesiowüstite. *Phys. Status Solidi B* 243:2111–16
- Tsuchiya T, Wentzcovitch RM, da Silva CRS, de Gironcoli S. 2006b. Spin transition in magnesiowüstite in Earth's lower mantle. *Phys. Rev. Lett.* 96:198501
- Verma AK, Modak P, Stixrude L. 2018. New high-pressure phases in MOOH ( $M = \text{Al, Ga, In}$ ). *Am. Mineral.* 103:1906–17
- Wade J, Wood BJ. 2005. Core formation and the oxidation state of the Earth. *Earth Planet. Sci. Lett.* 236:78–95
- Wallace DC. 1972. *Thermodynamics of Crystals*. New York: John Wiley
- Wang X, Tsuchiya T, Hase A. 2015. Computational support for a pyrolitic lower mantle containing ferric iron. *Nat. Geosci.* 8:556–59
- Wang X, Tsuchiya T, Zeng Z. 2019. Effects of Fe and Al incorporations on the bridgmanite–postperovskite coexistence domain. *C. R. Geosci.* 351:141–46
- Weertman J. 1957. Steady-state creep through dislocation climb. *J. Appl. Phys.* 28:362–64
- Wentzcovitch RM, Karki BB, Cococcioni M, de Gironcoli S. 2004. Thermoelastic properties of  $\text{MgSiO}_3$ -perovskite: insights on the nature of the Earth's lower mantle. *Phys. Rev. Lett.* 92:018501
- Wentzcovitch RM, Tsuchiya T, Tsuchiya J. 2006.  $\text{MgSiO}_3$  postperovskite at  $D''$  conditions. *PNAS* 103:543–46
- Yu YG, Wentzcovitch RM, Tsuchiya T, Umemoto K, Weidner DJ. 2007. First principles investigation of the postspinel transition in  $\text{Mg}_2\text{SiO}_4$ . *Geophys. Res. Lett.* 34:L10306
- Zhao D. 2004. Global tomographic images of mantle plumes and subducting slabs: insight into deep Earth dynamics. *Phys. Earth Planet. Inter.* 146:3–34